ARL-TR-10194 ● Sep 2025

High-Temperature, High-Speed Testing of Silicon Carbide

by Natasha Bradley, Andrew J. Wright, David Lee, Kristopher D. Behler, Michael J. Presby, Todd Henry, and John Hrynuk

DISTRIBUTION STATEMENT A. Approved for public release: distribution unlimited.

NOTICES

Disclaimers

The findings in this report are not to be construed as an official Department of the Army position unless so designated by other authorized documents.

Citation of manufacturer's or trade names does not constitute an official endorsement or approval of the use thereof.

Destroy this report when it is no longer needed. Do not return it to the originator.

ARL-TR-10194 ● SEP 2025

High-Temperature, High-Speed Testing of Silicon Carbide

Natasha Bradley, Andrew J. Wright, Kristopher D. Behler, Todd Henry, and John Hrynuk
DEVCOM Army Research Laboratory

David Lee
Naval Air Systems Command (NAVAIR)

Michael J. Presby
NASA Glenn Research Center

DISTRIBUTION STATEMENT A. Approved for public release: distribution unlimited.

REPORT DOCUMENTATION PAGE

1. REPORT DATE	2. REPORT TYPE	3. DATES COVERED START DATE	END DATE
September 2025	Technical Report	March 2021	October 2022

4. TITLE AND SUBTITLE
High-Temperature, High-Speed Testing of Silicon Carbide

5a. CONTRACT NUMBER	5b. GRANT NUMBER	5c. PROGRAM ELEMENT NUMBER
5d. PROJECT NUMBER	**5e. TASK NUMBER**	**5f. WORK UNIT NUMBER**

6. AUTHOR(S)
Natasha Bradley, Andrew J. Wright, David Lee, Kristopher D. Behler, Michael J. Presby, Todd Henry, and John Hrynuk

7. PERFORMING ORGANIZATION NAME(S) AND ADDRESS(ES)	8. PERFORMING ORGANIZATION REPORT NUMBER
DEVCOM Army Research Laboratory ATTN: FCDD-RLA-VB Aberdeen Proving Ground, MD 21005	ARL-TR-10194

9. SPONSORING/MONITORING AGENCY NAME(S) AND ADDRESS(ES)	10. SPONSOR/MONITOR'S ACRONYM(S)	11. SPONSOR/MONITOR'S REPORT NUMBER(S)

12. DISTRIBUTION/AVAILABILITY STATEMENT
DISTRIBUTION STATEMENT A. Approved for public release: distribution unlimited.

13. SUPPLEMENTARY NOTES
ORCIDs: Natasha Bradley, 0009-0003-0635-8361; John Hrynuk, 0000-0002-3199-1332

14. ABSTRACT
This work presents an assessment of using temperature and jet velocity as metrics for repeatable high-temperature, high-speed testing of silicon carbide. In order to better understand the variability between different experimental setups, mounting, and boundary conditions, two different erosion setups were used. Tests were conducted at NASA Glenn Research Center, where erosion was observed. Testing was also conducted in a similar test facility at ARL with different sample mounting conditions. Silicon carbide test samples were fabricated in combination with boron carbide and alumina into 38.1-mm-diameter disks at thicknesses of 3.33 and 9.91 mm. Samples were then exposed to a high-temperature (~1371 °C), high-speed (150 m/s) flow for at least 60 min. To induce erosion of the silicon carbide, 50-µm alumina particles were added to the flow, while particle image velocimetry was used to characterize the flow speed and direction. Erosion was observed to be highly sensitive to the flow boundary conditions and test setup. When the erosion jet exit was extremely close to the sample, like in the High Velocity Burner Test Rig at NASA Glenn, the surface of the silicon carbide was worn smooth revealing void content from the manufacturing process inside the sample. In the ARL Jet Burner Test setup, the silicon carbide did not erode, despite similar jet velocities and temperatures. Particle image velocimetry data showed that jet expansion with distance and sample mounting condition is critical to the erosion process. The results of this report clearly demonstrate that jet velocity and temperature are insufficient variables to define erosion conditions, and boundary conditions play a critical role in the process. The results shown here highlight the need for the research community to develop a set of highly repeatable boundary conditions, and other experimental conditions, to accurately assess ablation and erosion processes of materials.

15. SUBJECT TERMS
high-temperature flows, erosion, high-speed flows, particle image velocimetry, silicon carbide, Mechanical Sciences

16. SECURITY CLASSIFICATION OF: a. REPORT	b. ABSTRACT	C. THIS PAGE	17. LIMITATION OF ABSTRACT	18. NUMBER OF PAGES
UNCLASSIFIED	UNCLASSIFIED	UNCLASSIFIED	UU	27

19a. NAME OF RESPONSIBLE PERSON	19b. PHONE NUMBER *(Include area code)*
Natasha Bradley	(520) 691-5798

STANDARD FORM 298 (REV. 5/2020)
Prescribed by ANSI Std. Z39.18

Contents

List of Figures

List of Tables

Acknowledgments

This work, supported by ARL and the NASA Glenn Research Center, was accomplished under cooperative agreement number W911NF-19-2-0197. The views and conclusions contained in this document are those of the authors and should not be interpreted as representing the official policies, either expressed or implied, of ARL or the U.S. Government. The U.S. Government is authorized to reproduce and distribute reprints for Government purposes notwithstanding any copyright notation herein.

1. Introduction

High-performance aircraft, specifically high-temperature, high-speed (HTHS) systems, have driven new requirements for aviation materials and a need to develop reliable test methods for evaluating material performance in-situ. HTHS material characterization presents unique challenges for data collection. Reaching the high-flow velocities and temperatures needed to degrade the material limits, many traditional material testing techniques, like digital image correlation, cannot be used to correctly analyze the results. In some cases, the flow conditions cause the underlying material to deteriorate by ablation or erosion. During ablation, a material can be vaporized or dissolved when high heat is applied,[1] whereas during erosion, the material is worn or chipped away,[2] but this can occur in the same HTHS environment. Hot particulate ingestion rigs provide a unique capability for testing materials and components at conditions similar to those found in the combustion section of the turbine. These are often referred to as "burner rig"[3] or "hot torch"[4] systems and are designed to generate a high temperature and velocity flame using a combustor with a contracting nozzle, similar to a low-speed wind tunnel. Typical operating conditions for this type of equipment are temperatures of approximately 1300 °C at flow speeds of Mach 0.3,[5] but temperatures and velocities can be pushed to 1600 °C or Mach 0.8, respectively.[6] Extensive research has been carried out using these systems, primarily focusing on thermal cycling and corrosion effects of various thermal barrier coatings when contaminants such as sand or ash are intentionally added to the combusted flame.[3,7–9] However, these systems have also been used to study the oxidation of metals and ceramics, and to test the thermomechanical behavior of ceramic matrix composites.[10–12] A few studies on silicon carbide (SiC) have been conducted using burner rig systems to examine the oxidation and thermal cycling behavior of that material.[13–15]

SiC is of particular interest in HTHS applications due to its high-temperature resistance, low weight, beneficial mechanical properties, and ablation resistance.[16,17] SiC has been shown to retain its strength at temperatures in excess of 1500 °C and retains its fracture toughness.[18] SiC also provides oxidation resistance in air at temperatures in excess of 1700 °C, making it an ideal material for high-temperature applications.[19] It is a favored material as a matrix for reinforcing fiber in SiC–SiC or carbon fiber–SiC composites[20] and is commonly used in ultra-high temperature composite (UHTC) blends due to its ability to form lower temperature eutectics, improve sinterability, and reduce the overall weight of the UHTC while improving mechanical properties such as strength, most notably in zirconium and hafnium carbide and diborides.[21–24]

While SiC has a wide range of applications, the required conditions for ablation or erosion of SiC are of interest for the current study. Different methods of ablating SiC samples have been shown to result in different minimum ablation temperatures. When using an oxyacetylene flame, the ablation of a C/SiC material has been shown to occur at temperatures above 2000 °C.[4] Although the density and methods used to create the material have some effect on the variance seen in the ablation temperatures, there is also variance using similar techniques with an oxyacetylene flame. Research using plasma spraying, which is the injection of erosion particles with a plasma jet, showed ablation temperatures in excess of 3000 °C.[25] In some cases, the use of an air-based plasma can cause ablation below 2000 °C,[26] but this lower ablation temperature was caused by a geometry change in the test sample. Studies using laser pulsing with an Nd/YAG millisecond pulsed laser at a wavelength of 1064 nm demonstrated SiC ablation at a wide range of temperatures, between 2700 and 3500 °C. However, in this case the laser was observed to be ablating the carbon in the sample that had not been converted into SiC during the sample generation process.[27] Erosion results are more variable than ablation because flow direction, temperature,[28] particle velocity, and distribution of particles[29] have been shown to change erosion rates. In SiC, erosion can occur at temperatures as low as 815 °C,[30] when high speeds and larger particles are present. The higher the temperature, the lower the particle size as the temperature weakens the material itself,[31] also impacting the erosion rate.

One key challenge in comparing the range of previous studies is the wide variety of experimental techniques used to generate SiC ablation or erosion. This study evaluates one aspect of the experimental methods for ablation of SiC, specifically the boundary conditions of high-speed jet-based erosion. Two methods for generating the erosion of an SiC sample are shown—one conducted at the U.S. Army Combat Capabilities Development Command (DEVCOM) Army Research Laboratory (ARL) and one at NASA Glenn Research Center—followed by a discussion of how best to characterize the erosion conditions of SiC. The results will show that fundamentally similar flow conditions, when characterized using the obvious metrics of flow speed and temperature, will produce drastically different erosion conditions. Flow-field results from particle image velocimetry (PIV) testing will be used to understand how the input flow conditions must be adequately matched to determine temperature and velocity combinations required for erosion or ablation. Finally, recommendations for improvements to testing standards will be discussed.

2. Experimental Methods

2.1 Materials and Fabrication

The SiC test samples used in this study were hot-pressed using an oxygen benchtop hot press. SiC powder (Kyocera UF15) was mixed with boron carbide (Hoganas HS) and alumina (Baikowsi A16) on a rolling milled with SiC milling media and ethyl alcohol, a basic ceramic armor mixture.[32] The dried powder was weighed and placed into a 38.1-mm-inner-diameter graphite die ensemble mold, forming small coin-shaped samples (Figure 1). Three thicknesses of sample discs were created: 9.91 mm labeled as "thick," 6.65 mm labeled as "intermediary," and 3.33 mm labeled as "thin." Thick samples were designed to enable measurement of the erosion process, where the material was expected to erode over time. The two thinner samples were designed to allow for some aero-structural deformation of the material. The size of the samples was selected to ensure that that majority of the samples would be covered by the jet flow produced by the test setups used, with an aim of reducing the temperature gradients on the outer edges. The sizes and weights of the samples are also shown in Table 1.

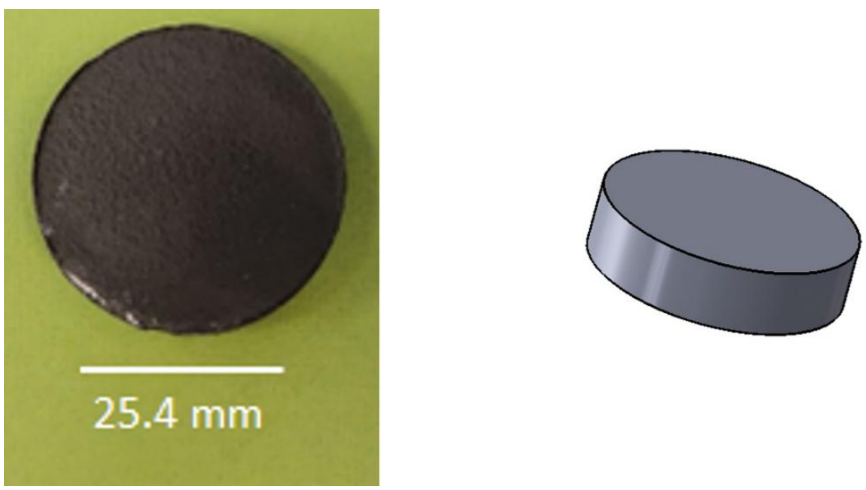

Figure 1. SiC puck with target as-pressed diameter and thickness dimensions of 38.1 and 9.91 mm, respectively.

Table 1. Sample parameters.

Test locations	Measurement		
	Thickness (mm)	Weight (g)	Diameter (mm)
ARL			
Thick sample	9.91	36.16	38.1
NASA Glenn			
Thin sample	3.33	10.12	38.1
Intermediary sample	6.65	22.67	38.1

2.2 High-Speed and Temperature Jet Flow for Erosion Testing

To better understand the variability between different experimental setups, mounting, and boundary conditions, two different erosion setups were used. Initial tests were conducted at NASA Glenn, where erosion was observed. Follow-on testing was conducted in a similar test facility at ARL with different sample mounting conditions. Table 2 shows the test conditions in the two experimental facilities, which are described in more detail in the sections below. The erosion jet velocity was held constant for all tests, as were the size and type of the eroding particles, but the temperature and eroding particle inflow rate varied slightly between facilities. While erosion was observed for both thick and thin samples at the NASA Glenn facility, erosion was not observed at the ARL facility despite comparable temperatures, jet velocity, and a higher eroding particle flow rate.

Table 2. Burner rig test times.

Test locations	Temperature (°C)	Flow speed (m/s)	Particle amount (g/min)	Time (h)
ARL				
Thick sample	982–1427	150	4.2	1
NASA Glenn				
Thick sample	1427	150	2.0	3
Intermediary sample	1315	150	2.0	3

2.2.1 High-Velocity Burner Test Rig at NASA Glenn

Initial erosion testing was conducted at the NASA Glenn Erosion Facility using the high-velocity burner rig shown in Figure 2. The erosion burner rig facility at NASA Glenn contains a jet burner with Mach 0.3–1.0 flow speed capability using Jet-A fuel and a preheated air mixture to accelerate the flow. A powder feeder (HA 5000 F-SA, Hardface Alloys, Inc.) was used to inject eroding particle material. This system sends 50-µm alumina through a feed line into the burner chamber, after which the particle-laden flow passes through a 19-mm-diameter nozzle where it is accelerated to 150 m/s. The speed and size of the particle were chosen to match the conditions tested at the ARL test rig.* A 305-mm-long duct is attached to the exit of the nozzle, carrying the particle flow out from the burner chamber to near the test sample. Samples were tested in this facility with flow temperatures of 1427 °C at 20-min intervals. After 20 min, the flame was turned off for 10 min to allow for measurement of the erosion process and imaging of the cooled sample. The test sample was clamped into a vice grip and placed at the end of the duct with a standoff

* The 50-µm particle size is found in the ASTM G76-13 standard for erosion by solid particle impingement[33] as a well-defined size because of its use.

distance of 3 cm from the duct exit. Figure 2 displays the burner exit nozzle, the unattached duct, and the vice grip with sample.

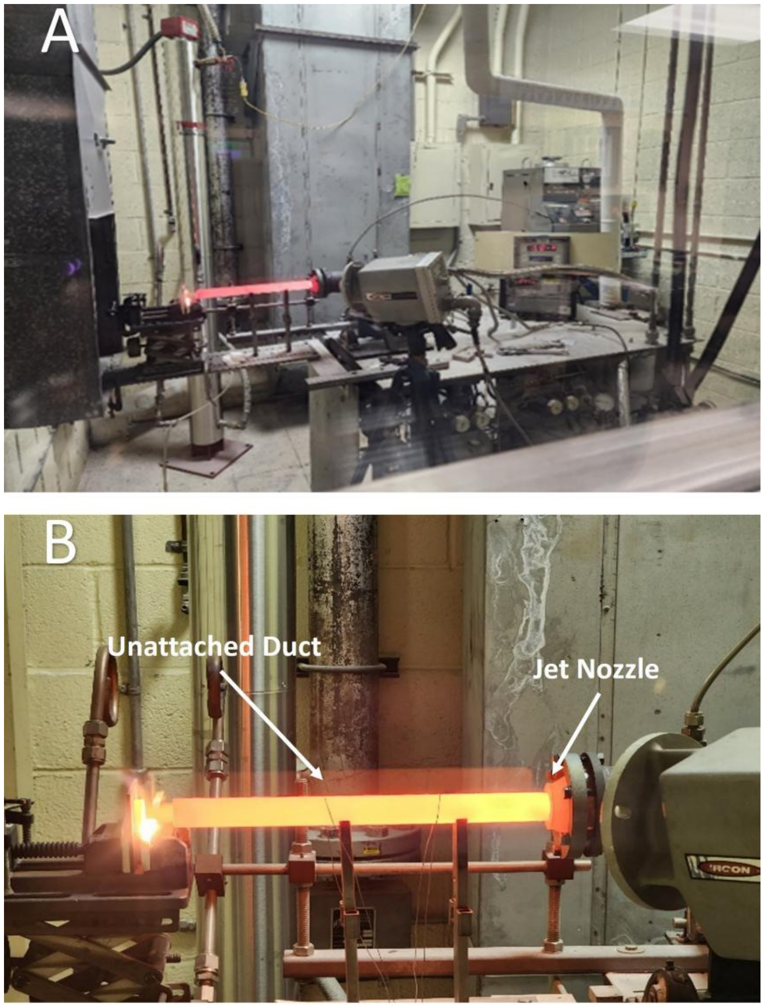

Figure 2. (A) High-velocity burner rig at NASA Glenn Erosion Facility located in NASA Glenn Research Center. (B) Close-up view of the burner rig with the nozzle and duct labeled.

2.2.2 ARL Jet Burner Test Setup

Additional tests were conducted using an open atmospheric HTHS flow generation system located in ARL's jet burner facility. A combusted-flame open-jet flow was generated by igniting jet fuel (F24[3]) in the combustor of the burner rig. Air and fuel are fed into the system near the back of the combustor with additional air fed into the system near the nozzle to generate turbulence and enhance mixing. Note that unlike the NASA Glenn Erosion Facility, the flame generated by the ARL combustor exited through a 5-cm nozzle, forming an open expanding jet that interacted with the SiC sample at a standoff distance of 20 cm. Care was taken to validate the flow speed and temperature at the sample mounting position, which aligned with testing at NASA Glenn. Most studies on erosion and ablation report an incoming flow speed only, so this difference was not expected to result in different erosion behaviors. As before, the sample was held tightly in a steel vice, which allowed for a fixed, repeatable positioning of the test samples. A type-R thermocouple, located radially 2 cm away from the nozzle, was used to measure the jet temperature at the center of the flame. Throughout the test the temperature ranged from 982 to 1427 °C. Two different experiments were conducted with each sample: one where the sample was entered directly into the flame and one where the location was the same but there was no flame, just compressed air blown from the rig controlled by pressure.

2.3 Particle Image Velocimetry (PIV)

PIV data was collected as part of the ARL testing (Figure 3). This test setup fed 50-µm alumina particles into the jet prior to combustion; the particles survived the combustion process and were used as the seed particles for PIV. Illumination of the PIV seed particles was done with an EverGreen HP ND-YAG dual-pulse laser aligned with the center line of the jet exit. Alumina was used due to its high refractive index, and early preliminary testing showed that the 50-µm size gave the best distribution of particles in the field of view (FOV). Each head of the laser has a maximum power of 200 mJ/pulse at 15 Hz. Image pairs were collected using Dantec FlowSence CV cameras with Dantec Dynamic Studio software for data collection. Optical band-pass filters at 532 nm were installed on the cameras to reduce the light from the flame. The cameras have 4-MP complementary metal-oxide semiconductor sensors with a resolution of 2336 × 1728 pixels for double-frame images up to 200 Hz. The resulting FOV of each camera was 43.4 × 27.1 cm. There was approximately 10% overlap between the two FOVs in the streamwise direction, creating a total FOV of 78.4 × 27.1 cm. Image pairs were collected with a delay time of $\Delta t = 0.225$ ms to maintain a maximum particle displacement between images of less than 7 pixels. The correlation window size was 16 × 16 or 18 × 18 pixels, depending on the case. The flow fields presented in this work are the time-average of 60 s of data to develop a sufficient average flow field for the highly turbulent jet.

For tests at high temperatures, the burner rig was allowed to reach steady temperatures, after which the feeder was turned on at a rate of 4 g/m and the sample was moved into the jet flow. Flow around the sample was allowed to stabilize for approximately 30 s before the PIV images were collected. For the room temperature, or "cold" tests, the same test process was used but without the need to allow the rig to stabilize at set temperatures.

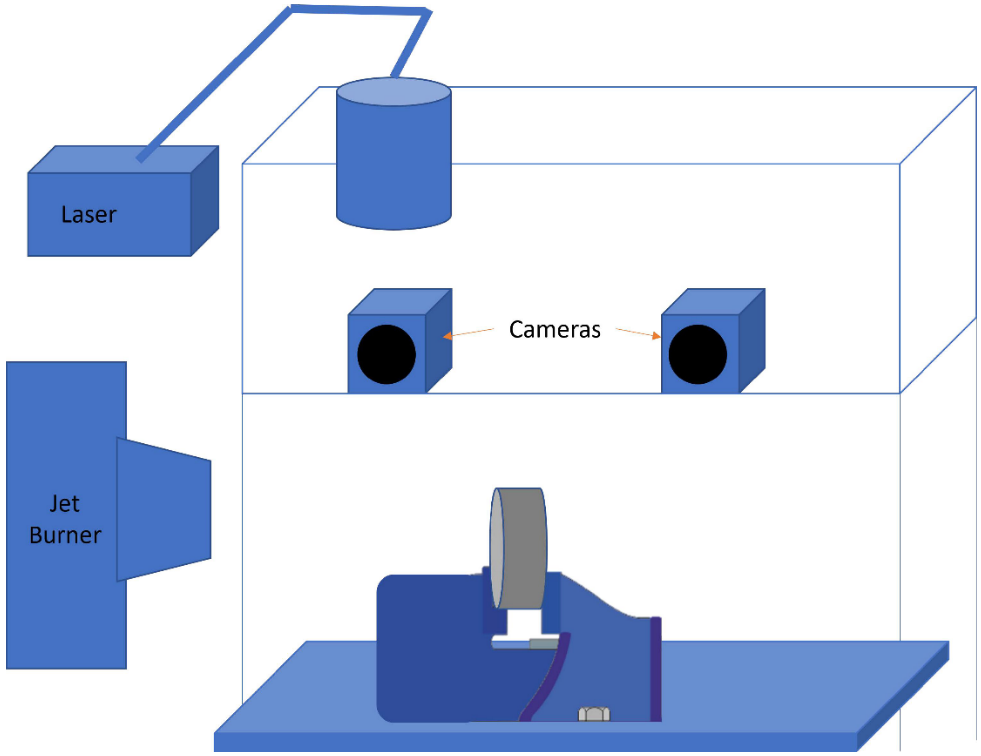

Figure 3. Side view of PIV test setup.

3. Results and Discussion

This section discusses the jet–sample interaction for both NASA Glenn and ARL test results. As noted previously, the tests at ARL did not result in erosion. Instead, the eroding particles collected on the sample resulting in an increased final mass. A discussion of the different boundary conditions will demonstrate the need for improved testing standards for erosion of HTHS materials.

3.1 NASA Glenn Erosion Testing

The test conditions of the NASA Glenn experiments were observed to be sufficient for erosion, with the erosion results shown in Table 3. Material was primarily lost by erosion caused by the alumina particles and not due to ablation, since ablation temperatures for the samples were not reached during the experiments. The samples were observed to erode as a function of time (Figure 4), with the bulk of the erosion occurring in the first 20 min of testing. After this initial erosion period, a slower, linear decrease in mass was observed through the remaining 160 min of testing. After the first inspection interval, initially rough surface of the samples had been smoothed significantly by the erosion process. At later inspection intervals, small voids were also observed forming on the surface (Figure 5b), which were likely present in the interior of the sample as part of the manufacturing process. As shown in Table 3, the mass loss trend of both the thin and thick sample was similar with final mass losses of 0.11 and 0.16 g, respectively. Confocal microscope measurements of the surface roughness are shown in Figure 4, where the erosion and smoothing of the surface can be easily observed. The average surface roughness, S_a, was found to decrease on the surface of the two samples tested from an initial 11.9 and 16.6 µm, to 4.2 and 4.8 µm after 3-h testing. Images of the full sample (Figure 5) show that the erosion was nonuniform. The circular eroded section suggests that despite the high temperature and speed of the jet, only a small center region resulted in erosion. The well-known studies by Livingood and Hrycak[34] and Gauntner[35] showed that the heat transfer profile of a jet impinging on a plate is Gaussian in nature, with high-heat transfer near the center of the jet decreasing significantly by approximately five nozzle diameters from the centerline of the jet. Similarly, it is shown in both Gauntner[35] and Livingood and Hrycak[34] that there are multiple jet interaction regions including, in order, flow establishment, development, deflection, and the wall jet region after the jet deflects outward. One key difference comparing this study to those is that the sample size was small relative to the jet diameter. While this would nominally suggest that the sample would be fully contained in the jet, the results shown in Table 3 suggest that the flow around the samples may be affecting the results. However, the results broadly suggest that this case reasonably aligns with a jet impinging on a wall, with the momentum clearly forced outward and a small region eroding in the process.

Table 3. Erosion results.

Sample size	Starting weight (g)	Posttest weight (g)	Material eroded (g)
ARL			
Thick sample	36.16	36.18	–0.02
NASA Glenn			
Thick sample	22.67	22.51	0.16
Thin sample	10.33	10.24	0.11

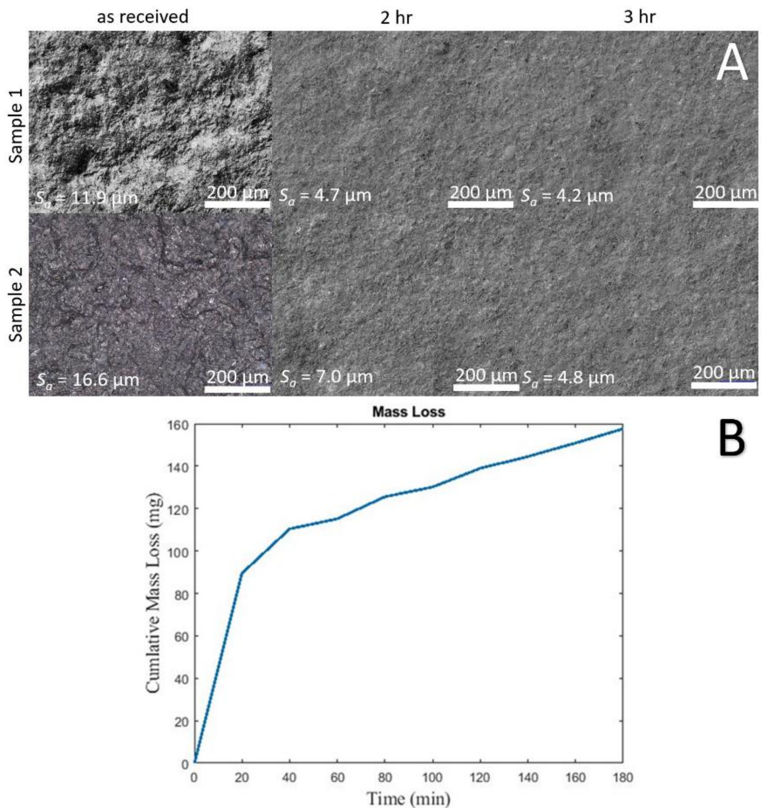

Figure 4. **Surface roughness measurements (A) and sample mass loss as a function of time due to alumina particle erosion via NASA Glenn high-velocity burner rig (B).**

Figure 5. **Sample images: (A) pretest; (B) post-120-min surface, NASA Glenn; and (C) post-60-min surface, ARL.**

3.2 ARL Testing

Despite similar jet temperatures and velocities, erosion was not observed on the samples tested at ARL. As observed in Figure 5, the alumina particles intended to aid in eroding the sample appear to have instead built up on the surface of the sample over time. At the end of testing, a layer of alumina was observed to build up on the mounting hardware, which flaked off upon removal of the sample. The buildup of particles on the sample occurred over a wider area than the erosion was observed for the NASA Glenn tests. This suggests that the size or spread of the jet, in the established flow region,[34,35] was larger in the ARL tests, which was expected. However, the measured jet velocity and temperature were comparable, which suggests that other factors affected the erosion process.

To investigate which factors are affecting the erosion process, PIV data was recorded for the ARL tests, including a cold-flow baseline with no combustion to study jet expansion due to temperature in the ambient room. A "hot" flow case was also recorded, with a combustor outlet temperature of 982 °C. The cold flow results with no sample installed are shown in Figure 6A, which expectedly resulted in significantly slower flow conditions than the combusted jet output. The mounting clamp for the sample was installed for all PIV testing to determine the jet velocity around the mounting hardware. While the jet flow was significantly decelerated for the cold flow case, there was not a significant deflection of the jet around the mounting hardware.

The experiment was then conducted with hot flow (Figure 6B) to assess the quality of the PIV measurements when the light from the jet burner was illuminating the sample. A filter was added to the PIV camera lenses to ensure that the cameras could clearly distinguish the alumina particles from the image background. The hot flow results were similar in appearance to the cold flow, with the jet near the sample having a diameter of around 10 cm. The velocity in the core of the jet measured using PIV was 150 m/s, which matches the speed of the particulates exiting the jet in the NASA erosion tests.

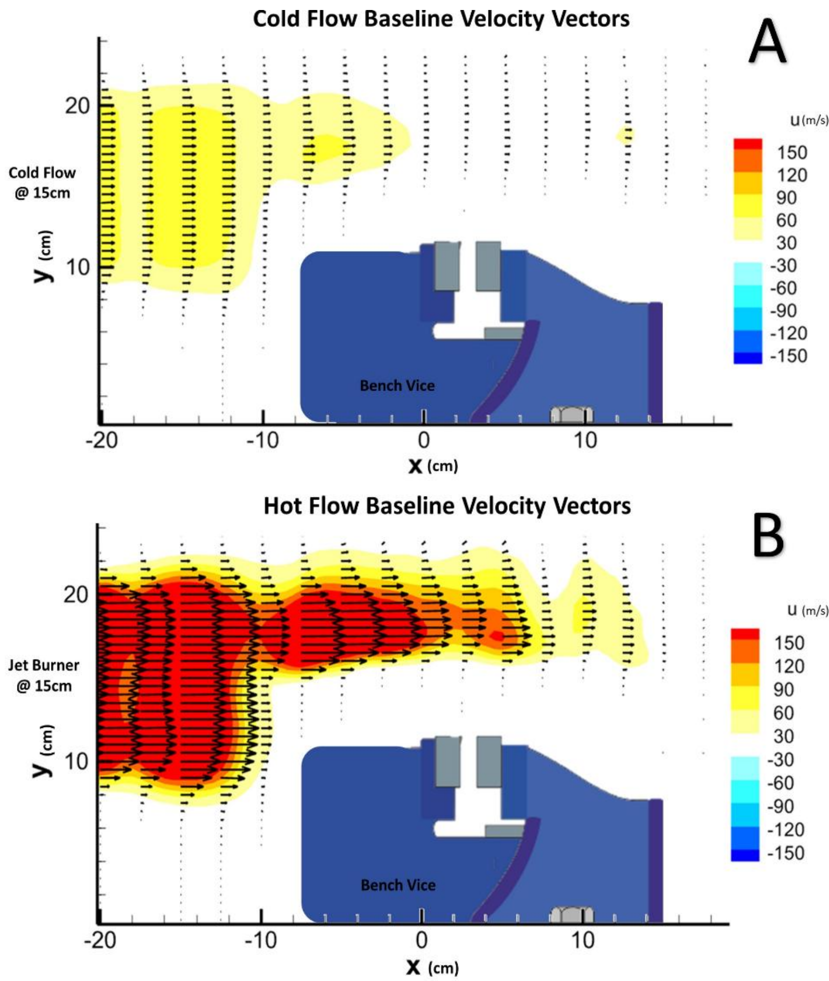

Figure 6. (A) Cold flow and (B) hot flow velocity measurements from PIV.

The flow field around the test samples is presented in Figure 7 for the cold flow and Figure 8 for the hot flow. In the cold flow (Figure 7) the jet was observed to directly impinge on the samples. There was a clear deflection of the jet upward around the sample and increasing jet velocity when the pressure settings of the burner rig were increased to the highest pressure (~150 m/s). As expected, there was no erosion observed for cold flows. Increasing the temperature of the jet altered the jet behavior, resulting in a slower jet in the high-velocity regions. In the worst case, this jet diffusion resulted in velocities near the sample of only 100 m/s. These flow field results clearly demonstrate that jet exit velocity and temperature are insufficient for setting erosion conditions in experiments.

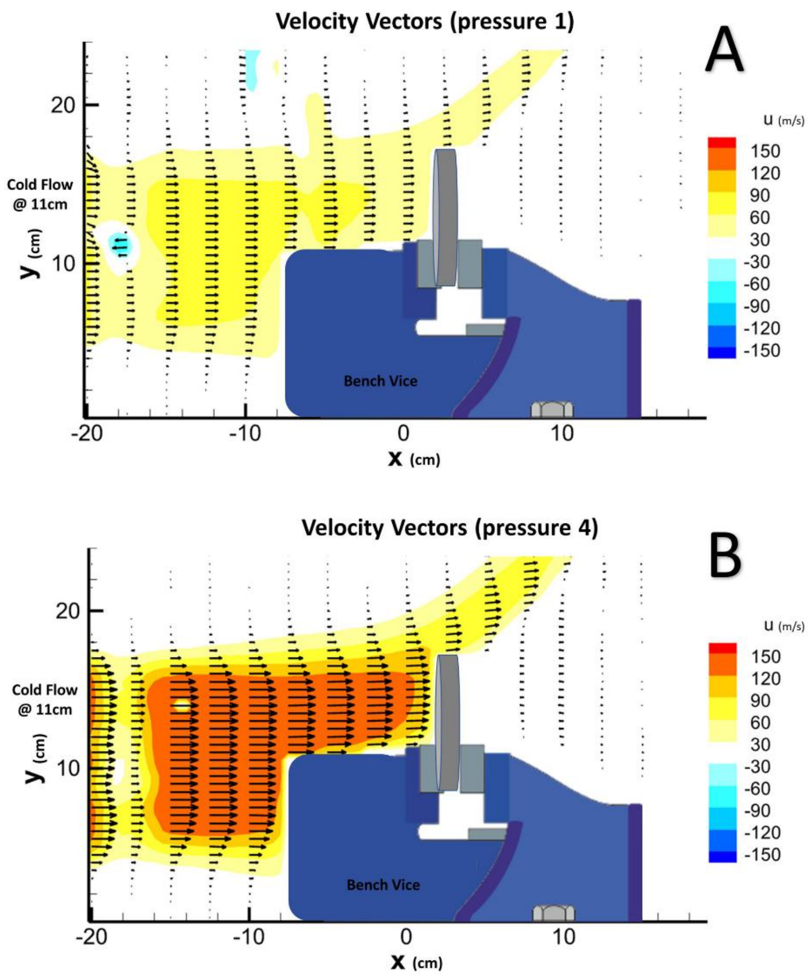

Figure 7. Cold flow visualization: (A) minimum and (B) maximum flow pressures.

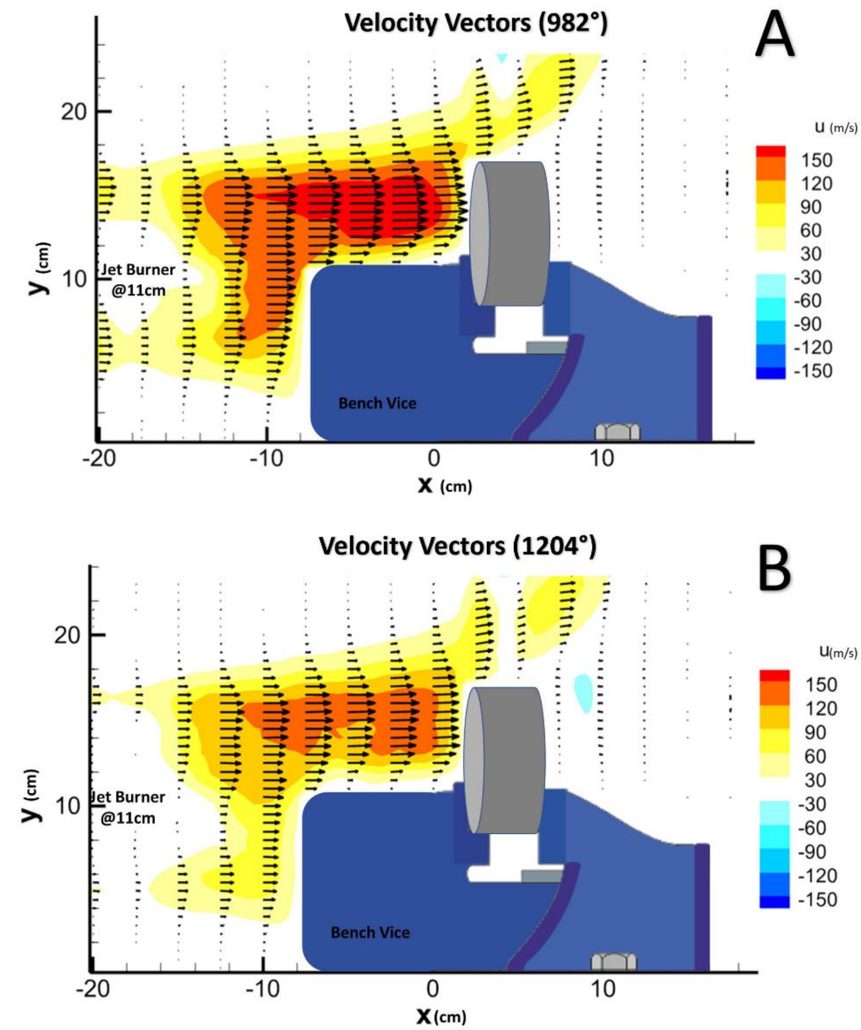

Figure 8. Hot flow visualization: (A) 982 °C and (B) 1204 °C.

The reason for the difference seen in the results shown in Figure 5, and also for the difference in the flow speed observed in Figure 8, is most likely due to the boundary conditions of the experimental setup. Figure 9 is presented to schematically describe the issues with variable flow boundary conditions in erosion and ablation experiments. Figure 9A-B schematically shows the experimental conditions in the ARL setup and the NASA Glenn setup, respectively. Allowing free expansion of the eroding jet into the quiescent air in the lab reduced the total velocity and ability of the jet to impart both momentum and temperature onto the samples. Focusing the jet and limiting the jet expansion, like during the NASA Glenn experiment, caused an erosion condition. Based on this, it becomes clear that the jet impingement conditions are critical for repeatable experiments. When the jet diameter is larger than the sample size, or has significant room to expand around the sample, it becomes less likely that erosion will occur. Jet velocity and temperature are clearly insufficient to characterize erosion in the lack of a well-defined criteria for jet impingement.

Figure 9C shows an ideal case where the sample size, relative to the jet diameter, is sufficiently large. This ideal case is confirmed with the NASA Glenn test, the jet diameter being smaller than the sample and leaving a small unaffected rim around the erosion area (Figure 5B). Therefore, it is recommended that either the sample diameter or surrounding mounting conditions have a length of at least two to three times the jet diameter of the incoming hot flow conditions. Close proximity of the impinging jet is also recommended to limit expansion, but more work is needed to identify sufficiently close conditions for the jet exit.

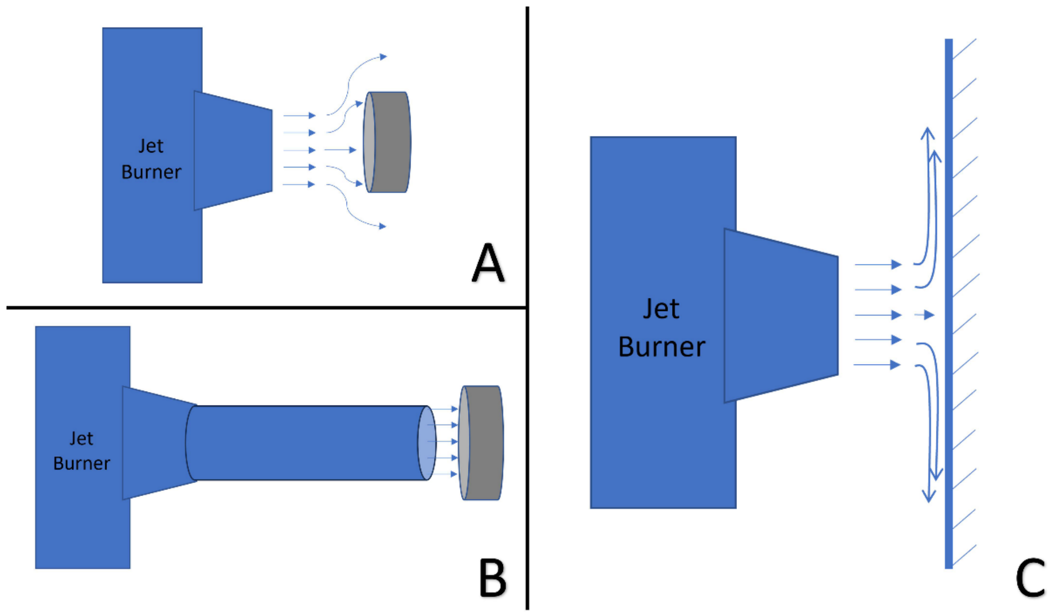

Figure 9. Boundary conditions of jet burner (A) at ARL, (B) at NASA, (C) with a wall plane.

4. Conclusions

SiC samples were tested in an HSHT environment intended to create erosion and ablation damage. In the NASA Glenn test, it was found that for temperature and speed combinations of around 1371 °C and 150 m/s, SiC would erode when the hot flow outlet was 1.9 cm in diameter with a standoff of 3 cm. In this configuration, the surface of the SiC was worn smooth from an S_a of 12–16 µm to a post-3-h S_a of 4–5 µm, revealing void content from the manufacturing process inside the sample. In the ARL setup, the SiC did not erode or abrade, but instead accumulated the particles meant to erode the sample. The exiting jet diameter of 5 cm expanded to around 10 cm near the samples, approximately 20 cm from the jet exit. Over this distance the alumina particles meant to interact with the sample were found to scatter as the hot flow column expanded in the room, resulting in much of the flow energy being directed away from the sample. Increasing the hot flow temperature and the amount of alumina in the flow did not lead to erosion.

Based on the observations in this study, the temperature and velocity of an impinging jet are not sufficient to define erosion conditions. The impinging jet expansion conditions, including standoff and the ratio of sample diameter to jet diameter, are critical for repeatable experiments in this space. The authors recommend the sample diameter be at least two to three times the jet diameter and that efforts be taken to minimize the standoff distance of the jet exit. Under these conditions, repeatable HSHT testing for erosion and ablation becomes more likely.

5. References

1. Tan W et al. Ablation behavior and mechanism of C/C-HfC-SiC composites. Vaccum. 2015;116;124–129.

2. Presby M. High-temperature solid particle erosion in a melt-infiltrated SiC/SiC ceramic matrix composite. Journal of Engineering for Gas Turbines and Power. 2021;143:1–15.

3. Walock M et al. Ceramic matrix composite materials for engine exhaust systems on next-generation vertical lift vehicles. Journal of Engineering for Gas Turbines and Power. 2018;140:1–15.

4. Wang T, Chen Z, Yu S. Ablation behavior and mechanism analysis of C/SiC composites. Journal of Materials Research and Technology. 2016;5:170–182.

5. Murugan M et al. Sand particle-induced deterioration of thermal barrier coatings on gas turbine blades. Advances in Aircraft and Spacecraft Science. 2017;4:37–52.

6. Nieto A et al. Calcia–magnesia–alumina–silicate (CMAS) attack mechanisms and roadmap towards sandphobic thermal environmental barrier coatings. International Material Reviews. 2021;66:451–492.

7. Sharma A, Witz G, LeCreux C, Hitchman N. High heat flux burner-rig testing of 8ysz thermal barrier coatings: Influence of the powder feedstock. Journal of the European Ceramic Society. 2022;42:7267–7274.

8. Gildersleeve EJ, Sampath S. Dynamic interactions of ingested molten silicate particles with air plasma sprayed thermal barrier coatings. Journal of Materials Research. 2020;35:2321–2334.

9. Mock C, Walock M, Ghoshal A, Murugan M, Pepi M. Adhesion behavior of calcia–magnesia–alumino–silicates on gadolinia-yttria-stabilized zirconia composite thermal barrier coatings. Journal of Materials Research. 2020;35:2335–2345.

10. Badini C et al. Cyclic oxidation in burner rig of TiAlN coating deposited on Ti-48Al-2Cr-2Nb by reactive HiPIMS. Ceramic International. 2017;43:5417–5426.

11. Smialek JL. Environmental resistance of a Ti2AlC-type max phase in a high pressure burner rig. Journal of the European Ceramic Society. 2017;37:23–24.

12. Yu Jet al. Corrosion behavior of CVI 2D Cf/SiC composites under high temperature burner rig tests. Corrosion Science. 2022;209:110596.

13. Baxter D, Bellosi A, Monteverde F. Oxidation and burner rig corrosion of liquid phase sintered SiC. Journal of the European Ceramic Society. 2000;20:367–382.

14. ZhongLiu W, Peng X, Zhuan L, XiaoYu Y, Yang L. Thermal cycling behavior and oxidation resistance of SiC whisker-toughened-mullite/SiC coated carbon/carbon composites in burner rig tests. Corrosion Science. 2016;106:179–187.

15. Ogbuji L. A pervasive mode of oxidative degradation in a SiC-SiC composite. Journal of the American Ceramic Society. 1998;81:2777–2784.

16. Wang X et al. Advances in modifications and high-temperature applications of silicon carbide ceramic matrix composites in aerospace: A focused review. Journal of the European Ceramic Society. 2021;41:4671– 4688.

17. Terrani K, Jolly B, Trammell M. 3d printing of high-purity silicon carbide. Journal of the American Ceramic Society. 2019;103:1575–1581.

18. Snead L et al. Handbook of SiC properties for fuel performance modeling. Journal of Nuclear Materials. 2007;371:329–377.

19. Hong J, Davis R, Newbury D. Self-diffusion of silicon-30 in α-SiC single crystals. Journal of Materials Science. 1981;16:2485–2494.

20. Yin X, Cheng L, Zhang L, Travitzky N, Greil P. Fibre-reinforced multifunctional SiC matrix composite materials. International Materials Reviews. 2016;62:117–172.

21. Carney C, Parthasarathy T, Cinibulk M. Oxidation resistance of hafnium diboride ceramics with additions of silicon carbide and tungsten boride or tungsten carbide. Journal of the American Ceramic Society. 2011;94:2600–2607.

22. Gasch M et al. Processing, properties and arc jet oxidation of hafnium diboride/silicon carbide ultra high temperature ceramics. Journal of Materials Science. 2004;39:5925–5937.

23. Rezaie A, Fahrenholz W, Gregory H. Evolution of structure during the oxidation of zirconium diboride–silicon carbide in air up to 1500 °C. Journal of the European Ceramic Society. 2007;27:2495–2501.

24. Monteverde F, Bellosi A. Microstructure and properties of an hfb2-SiC composite for ultra high temperature applications. Advanced Engineering Materials. 2004;6:331–336.

25. Wu H et al. Microstructures and ablation resistance of zrc coating for SiC-coated carbon/carbon composites prepared by supersonic plasma spraying. Journal of Thermal Spray Technology. 2011;20:1286–1291.

26. Yang L et al. New insights on the ablation mechanism of silicon carbide in dissociated air plasmas. Aerospace Science and Technology. 2022;129:107863.

27. Pan S, Li W, Xian Z, Su N, Zeng F. The effects of laser parameters and the ablation mechanism in laser ablation of C/SiC composite. Materials. 2019;12:3076.

28. Dorakr NV, Kim Y-W, BVM Kumar. Influence of temperature, impact angle and h-BN content on the erosive wear behavior of hot-pressed SiC-BN composites. Wear. 2020;458–459.

29. Hu Y, Pan J, Dai Q, Huang W, Wang X. Solid particle erosion-wear behaviour of SiC particle-reinforced Si matrix composite and neat Si—a comparison. Wear. 2022;496–497.

30. Abdollahi A, Valefi Z, Ehsani N. Erosion mechanism of ternary-phase SiC/ZrB2-MoSi2-Sic ultra-high temperature multilayer coating under supersonic flame at 90° angle with speed of 1400 m/s (Mach 4). Journal of European Ceramic Society. 2020;40:972–987.

31. Panakarajupally R et al. Solid particle erosion behavior of melt-infiltrated SiC/SiC ceramic matrix composites (CMCS) in a simulated turbine engine environment. Composites Part B: Engineering. 2021;216:108860.

32. Boldin M et al. Review of ballistic performance of alumina: Comparison of alumina with silicon carbide and boron carbide. Ceramics International. 2021;47:25201–25213.

33. ASTM G76-13. Standard test method for conducting erosion tests by solid particle impingement using gas jets. ASTM International; 2013.

34. Livingood JN, Hrycak P. Impingement heat transfer from turbulent air jets to flat plates: a literature survey. 1973.

35. Gauntner JW. Survey of literature on flow characteristics of a single turbulent jet impinging on a flat plate. 1970.

List of Symbols, Abbreviations, and Acronyms

ARL	Army Research Laboratory
DEVCOM	U.S. Army Combat Capabilities Development Command
FOV	field of view
HTHS	high-temperature, high-speed
NASA	National Aeronautics and Space Administration
PIV	particle image velocimetry
SiC	silicon carbide
UHTC	ultra-high temperature composite

1 (PDF)	DEFENSE TECHNICAL INFORMATION CTR DTIC OCA
1 (PDF)	DEVCOM ARL FCDD RLB CI TECH LIB